Thermal Protection System Models for Entry into Venus' Atmosphere

Grace Falanga, Ben Inbar, and Max Yasgur
Sibley School of Mechanical and Aerospace Engineering, Cornell University, Ithaca, NY 14850

NASA's Planetary Sciences Decadal survey expressed the need for an investigation of Venus' climate to increase our understanding of climate change on Earth. To do so, an in-situ explorer has been proposed that will use a semi-buoyant design in order to avoid the extreme temperatures and pressures on the surface of Venus. An investigation of the thermal protection system (TPS) requirements for this explorer to enter Venus' atmosphere was conducted using a number of NASA codes for simulating thermal conductivity of porous materials as well as heat flux loading and recession during atmospheric entry.

I. Nomenclature

AMAT	=	Aerocapture Mission Analysis Tool
C_b	=	Ballistic Coefficient
C_H	=	Stanton Number for Heat Transfer
h_e	=	Boundary Layer Edge Specific Enthalpy J kg^{-1}
h_w	=	Boundary Layer Edge Specific Enthalpy J K^{-1}
ISX	=	In-Situ Explorer
k_{eff}	=	Effective conductivity, W m^{-1} K^{-1}
k_{solid}	=	Effective solid conductivity, W m^{-1}
MSL	=	Mars Science Lab
P_t	=	Stagnation Pressure, Pa
PATO	=	Porous material Analysis Toolbox based on OpenFoam
PuMA	=	Porous Microstructure Analysis
q	=	Total Heat Flux, J m^{-2} s^{-1}
T	=	Temperature, K
TPS	=	Thermal Protection System
VCOAX	=	Venus Climate Orbiter and Autonomous Explorer
β	=	Optical extinction coefficient, m^{-1}
σ	=	Stefan-Boltzmann constant, W m^{-2} K^{-4}

II. Introduction

The 2013 - 2022 Planetary Sciences Decadal survey expressed the need for careful study of Venus' Climate as the only other example of a dense terrestrial planet atmosphere in our solar system. Venus with its greenhouse atmosphere has the potential to increase our understanding of climate change and its potential effects on our own planet [1]. The Venus Climate Orbiter and Autonomous Explorer aims to address this particular need of the scientific community by placing a highly capable orbiter around Venus as well as deploying an autonomous semi-buoyant helicopter to study the atmosphere and landscape of Venus in-situ.

The in-situ explorer will build on the success of the Mars Ingenuity helicopter that was a part of the Mars 2020 mission. Ingenuity demonstrated that not only could a rotor aircraft be flown extra-terrestrially, but that such a device could have significant value to a mission. Ingenuity far exceeded expectations in an environment that makes flying a helicopter extremely difficult. Venus on the other hand has a much more favorable environment for rotor aircraft, with a much denser atmosphere that significantly expands what a helicopter could accomplish.

One of the main challenges of sending a device such as a rover to the surface of Venus is engineering it to survive the extreme temperatures and pressures that are found on the surface. By utilizing an airship, the ISX will be able to avoid those engineering challenges. ISX will be a flying instrument platform capable of sampling and analyzing Venus'

atmosphere, weather patterns and climate dynamics using an on board suite of instruments [1]. It will also include ground sensing instruments in order to look for evidence of hydrological cycles, past life and evidence of oceans on the surface. The mission will set a minimum possible altitude for ISX below which the pressure will be too great for it to descend.

ISX will follow much of the same path as the two most recent Mars missions. The vehicle will be protected by an aeroshell comprised of a backshell and heatshield. The backshell will use the same SLA-561V cork ablative TPS material which is also a heritage material. The analysis of the backshell TPS, is not the subject of this study and will not be discussed further. Once the aeroshell has slowed from hypersonic to supersonic entry and the entry capsule has moved through peak heating, a supersonic parachute will be deployed, and the backshell and heatshield detached. ISX will then inflate it's balloon to maintain a nominal 50km altitude at the end of entry.

III. Methods

A. Orbital Mechanics

To determine a viable set of initial conditions for the entry profile, the orbital transfer from Earth to Venus was calculated using MATLAB. To begin, the NASA Ames Research Center Trajectory Browser was used to shrink the search space of departure and arrival times as well as provide estimates on the change in velocity, referred to as Δv, required to inject into the orbital trajectory. A local optimum trajectory was chosen with Earth departure on Dec-04-2024, injection Δv of 3.74 km/s, Venus arrival on May-29-2025, and C_3 capture burn of 432 m/s. These transfer parameters were then used to inform a constrained minimization problem such that the spacecraft minimized its arrival distance with Venus under a set of physical and cost constraints: the departure occurs outside of the Earth's sphere of influence and the injection Δv is less than 10 km/s. This constrained minimization was performed via MATLAB's fmincon operating on a numerical integration of the equations of motion using Cowell's method in MATLAB's ode113. The resulting Earth-Venus transfer can be seen in Fig. 1a. The transfer is a hyperbolic flyby of Venus (e=1.0028), therefore a retrograde capture burn must be applied to close the orbit. Modeling after the Venus Express mission, an initial pericytherion altitude of 460 km and apocytherion altitude of 63,000 km were selected, so another retrograde burn is applied at closest approach to achieve this intermediate orbit, which is shown in Fig. 1b. Lastly, a large 1.3 km/s burn is conducted at periapsis to bring the apoapsis from an altitude of 63,000 km down to 220 km, the atmospheric interface altitude, as shown in Fig. 1c. The final state vector was then transferred from MATLAB to AMAT, where the entry profile is calculated.

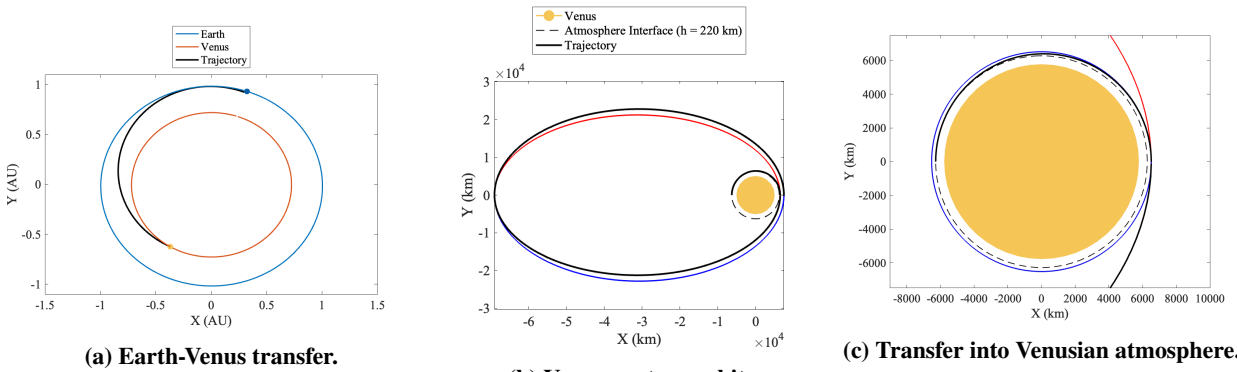

(a) Earth-Venus transfer.

(b) Venus capture orbit.

(c) Transfer into Venusian atmosphere.

Fig. 1 Orbital mechanics transfer sequence from Earth into the Venusian atmosphere. Subfigures (b) and (c) are presented in Venus' perifocal reference frame. Venus is not shown to scale.

B. AMAT

In order to be able to effectively model the thermal response of the VCOAX heatshield using PATO, a model of the entry profile was first needed. AMAT, a JPL and Purdue University code used to perform mid-fidelity aerocapture and atmospheric entry analysis, was identified as the most useful software package for this application [2]. For this

Table 1 MSL and derived ISX Aerodynamic Properties for use in AMAT Simulations. [3–5]

	MSL	ISX
Mass [kg]	3893	1881.02
C_b	140	140
$\frac{L}{D}$	.24	.24
A_{ref}	15.90431	3.976
Nose Radius [m]	1.125	.5625
Radius [m]	2.25	1.125

study, AMAT was used to generate the stagnation point heat flux and stagnation pressure along the entry trajectory. This effectively gives a 1D approximation of the entry heating profile of the capsule, which can then be passed to PATO.

AMAT allows the specification of a number of important geometric characteristics of the entry vehicle. Since ISX's aeroshell is derived from the MSL/Mars 2020, many of its aerodynamic characteristics remain the same. Table 1 outlines those characteristics for both MSL/Mars 2020 and ISX. The aerodynamic characteristics that were changed from MSL were calculated in an assignment for another class in order to meet the mission requirements, accounting for instrumentation and other hardware.

The resulting trajectory of this simulation can be seen in Fig. 2. The Stagnation pressure and heat flux were then passed into PATO as described in Section III.C.

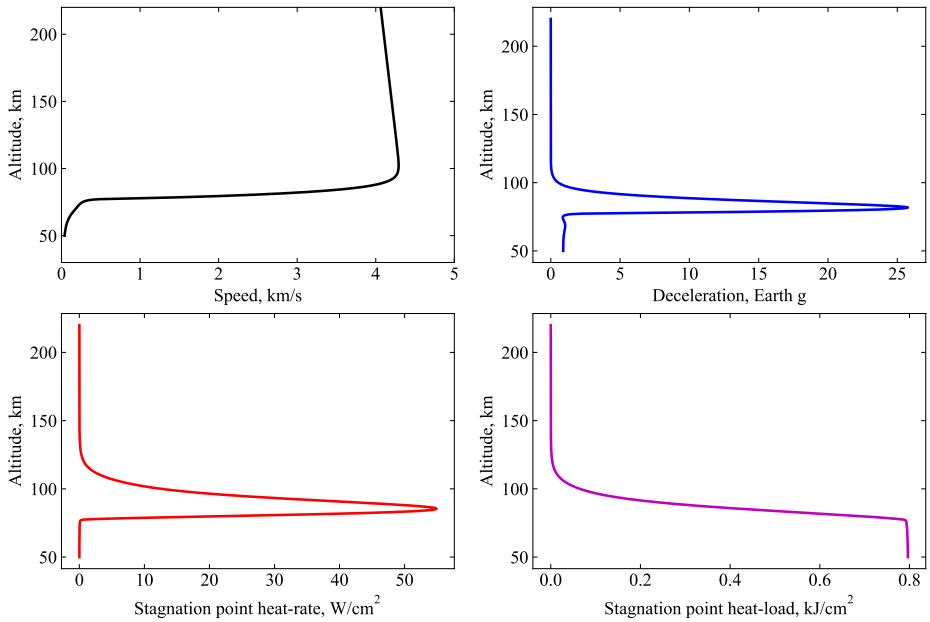

Fig. 2 Results of AMAT simulation of VCOAX Venus entry profile.

It is important to note that AMAT is a lower fidelity model than PATO, as it is only a 1D model of the system. This can be seen in Fig. 3 where AMAT is predicting roughly half of what PATO calculates. For a final design, a full-force, hypersonic CFD analysis would need to be done on the entry capsule, but as a starting point for mission planning, AMAT's approximations are good enough.

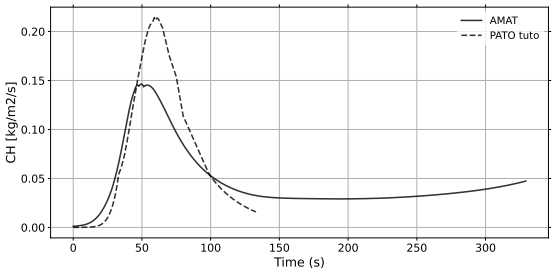

(a) Stanton Number for Heat Transfer as calculated by PATO and AMAT.

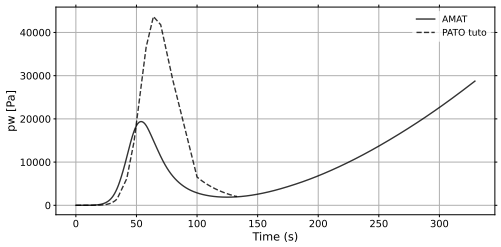

(b) Stagnation pressure as calculated by PATO and AMAT.

Fig. 3 Stardust Test Case Stanton Number for Heat Transfer and Stagnation Pressure from PUMA and PATO.

C. PATO

The stagnation point heat loading and pressure from AMAT was used as the boundary conditions in simulations of the heat shield ablation. These simulations were run using PATO, a NASA Ames code used to model the thermal response of porous thermal protection systems [6]. PATO allows the estimation of TPS internal temperatures and modelling of TPS recession. This allows the determination of TPS thickness by monitoring the bondline temperature and ensuring that it does not exceed the debonding temperature. In order to make the AMAT simulation results integrate into PATO, a code provided by Jeremie Meurisse at NASA Ames was implemented.

Once the AMAT-PATO integration was implemented, the thickness of the heat shield was specified in `blockMeshDict`, and the material in `constant/porousMat/porousMatProperties`. As the thickness was changed, TC locations were also updated in `system/porousMat/plotDict`. Starting with TACOT, as it is based on PICA and is a well-established heat shield for atmospheric entry, the minimum thickness required to remain under the maximum bondline temperature requirement was determined. From there, that minimum thickness was used in simulations with a carbon fiber preform without phenolic resin, a cork ablator, and a novel material based on fiberglass and modeled in PuMA to get thermal conductivity.

D. PuMA

In order to investigate materials not implemented as defaults in PATO, an effective conductivity needs to be calculated. This can be done using the NASA code, Porous Microstructure Analysis (PuMA) [7, 8]. In PuMA, a `.tif` file can be imported, and PuMA will utilize greyscale thresholding to decide which voxels are solid and which are void space. From there, the conductivity of the solid and void phases can be assigned separately, and PuMA will compute the effective conductivity of the composite material based on the geometry of both phases.

In this investigation, fiberglass was investigated as a replacement material to develop the workflow and serve as a proof of concept. Fiberglass is a commonly used reinforcing matrix in applications where carbon fiber is also used, which is why it was chosen. In an actual ablative heat shield applications, fiberglass may not be as helpful because it is not carbon-based, so it will not char, but it has a comparable density to carbon fiber, so it would still be light. In order to calculate the effective conductivity of the new heat shield material, a reference for the thermal conductivity of fiberglass over a range of temperatures was used, as shown in Fig. 4. The values for a density of 12 kg/m^3 were chosen. It is important to acknowledge that these results are actually effective conductivity of fiberglass insulation, which also includes air, which is why the densities are so low. In order to demonstrate the general workflow, however it was deemed sufficient to use these values. Given more time and resources, the conductivity of the solid phase could be experimentally determined as a function of temperature.

In PuMA simulations, the effective isotropic thermal conductivity was calculated over a range of temperatures by inputting each of the extrapolated conductivity values for fiberglass as the conductivity of the solid phase, using the FiberForm geometry from the PuMA examples. The conductivity of the void phase was taken as a constant value of 0.2 W/m-K, which is an determined value for phenolic resin [10].

The isotropic conductivity solver in PuMA was used to determine the effective solid conductivity contribution to the overall thermal conductivity, however this cannot be directly inputted into PATO as it does not account for radiation. At the high temperatures being considered, radiation will start to have a much larger impact on the thermal conductivity,

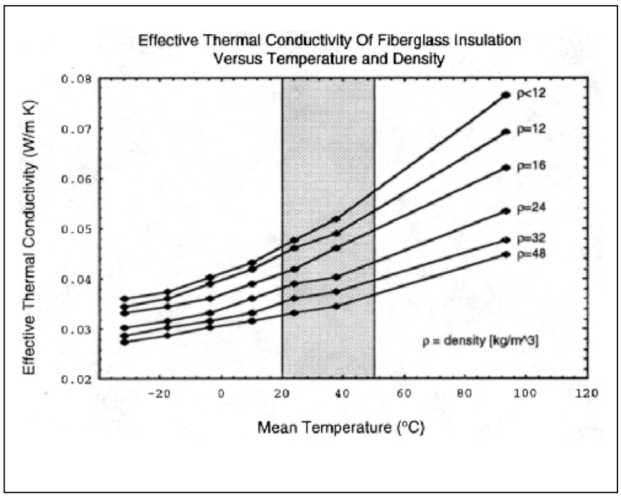

Fig. 4 Effective thermal conductivity of fiberglass insulation over a range of temperatures [9].

according to Eq. 1:

$$k_{\text{eff}} = k_{\text{solid}} + \frac{16\sigma}{3\beta}T^3 \tag{1}$$

The effect of radiation on conductivity can be calculated using a solver in `pumapy`, however the documentation was somewhat limited and there may be a bug in the code. As a result, an approximate value of the extinction coefficient, β from literature for carbon porous materials was chosen at 10 mm^{-1}. After calculating the effective conductivity according to Eq. 1, these values were put into a new material file and run in PATO. Isotropic conductivity was assumed, so each direction was given the same value of thermal conductivity. Additionally, based on the limited data, the heat capacity and enthalpy values were taken to be constant, and the emissivity and reflectivity were left as those of TACOT. Since fiberglass is much more transparent than carbon fiber this assumption is likely not valid, so future work would need to determine what the actual values of emissivity and reflectivity are.

Finally, the data for effective thermal conductivity of fiberglass was over a very small and low temperature range compared to what it would experience during atmospheric entry. Since PATO can only interpolate and will not extrapolate, some liberties needed to be taken in order to create a material file that would run. In a real simulation, of course, experimental data would be robust and would cover the full range of temperatures, but due to the limited resources and time the conductivity data was linearly extrapolated based on the data in Fig. 4 in order to create a comprehensive material file that could be run in PATO.

IV. Results & Discussion

A. Determination of Minimum Thickness with TACOT

Using the AMAT to PATO workflow presented in Sections III.B & III.C the thickness of the heatshield was varied until the maximum bondline temperature exceeded 500 K. This bondline temperature maximum was chosen based off of the MSL maximum bondline temperature of 250 °C [11]. 500 K was arbitrarily chosen as it is a round number near the 250 C limit.

The material thickness was incrementally reduced by 1 cm from 5 to 2 cm where the maximum temperature was exceeded. Further refinement in the simulations resulted in a minimum thickness of 2.75 cm which resulted in a maximum bondline temperature below 500 K, as shown in Fig. 5a. With TACOT and the entry profile calculated, the heat shields receeds less than 4 mm, leaving all of the thermocouples intact, as depicted in Fig. 5b.

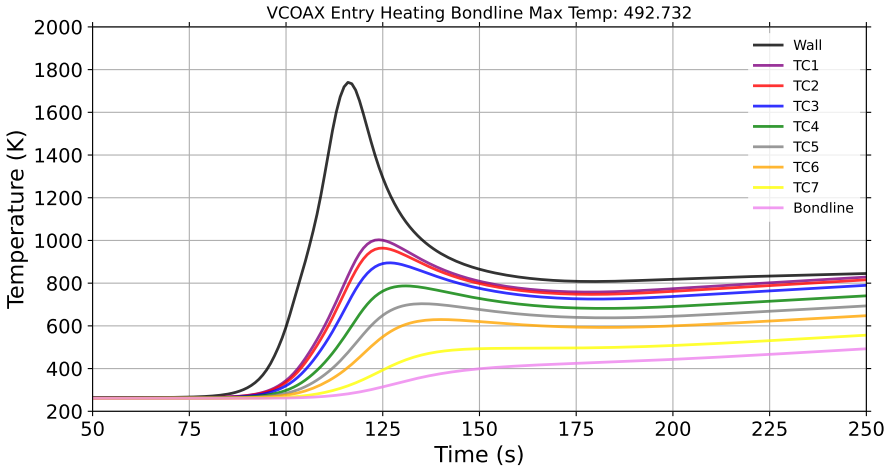

(a) Temperature profile of a 2.75 cm thick TACOT heatshield during Venus Atmospheric Entry. The thermocouples are placed at depths of 1.5599, 1.5965, 1.6696, 1.8159, 1.9622, 2.1085, and 2.401 cm from the surface of the heatshield. The boundary condition and bond line temperature are also plotted.

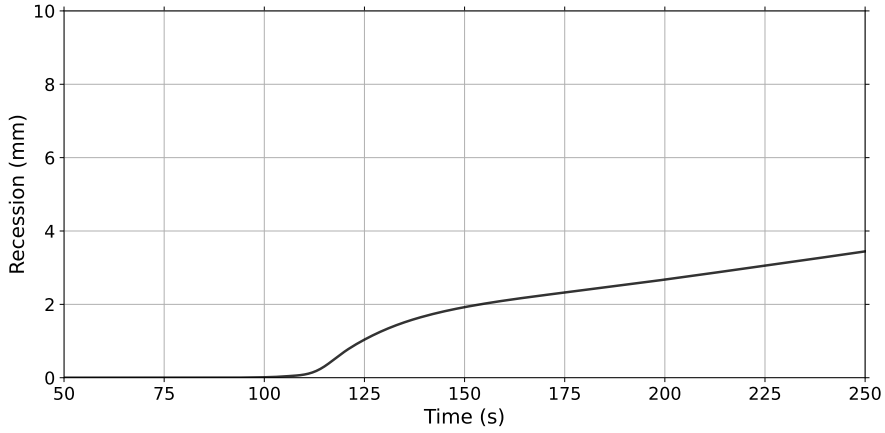

(b) Recession of a 2.75 cm heatshield during Venus Atmospheric Entry.

Fig. 5 Performance of a TACOT heat shield during Venus atmospheric entry showing (a) temperature and (b) recession.

B. Alternative Materials

1. Carbon Fiber Preform

The Carbon Fiber Preform material is TACOT without the phenolic resin included in it. We would expect to see a higher total temperature due to the lack of phenolic cooling of the material, which is confirmed by the simulation in Fig. 6a. We also see a higher bondline temperature, which slightly exceeds our maximum value as expected. The recession profile is slightly altered as well, with a greater total recession depth.

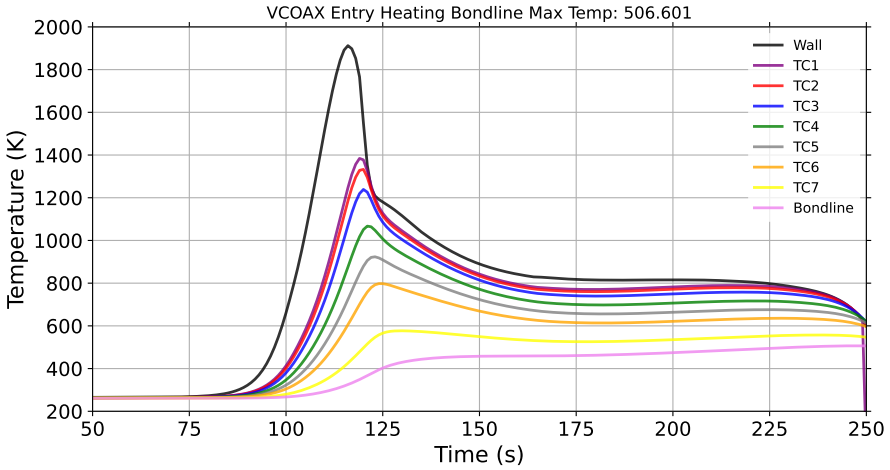

(a) Temperature profile of a 2.75 cm thick Carbon Fiber Preform heatshield during Venus Atmospheric Entry. The thermocouples are placed at depths of 1.5599, 1.5965, 1.6696, 1.8159, 1.9622, 2.1085 and 2.401 cm from the surface of the heatshield. The boundary condition and bond line temperature are also plotted.

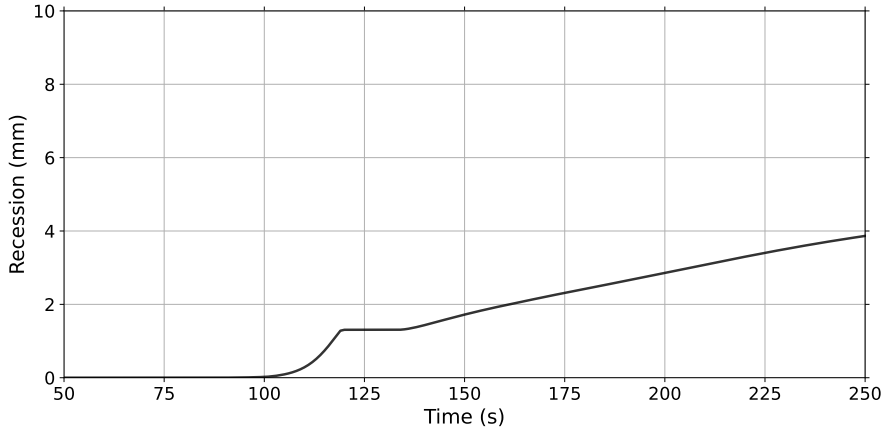

(b) Recession of a 2.75 cm thick Carbon Fiber Preform heatshield during Venus Atmospheric Entry.

Fig. 6 Performance of a carbon fiber preform (without phenolic resin) during Venus atmospheric entry showing (a) temperature and (b) recession.

2. Cork (No Pyrolysis)

The results show that entry-level heating of cork without pyrolysis effects shows noticeably lower recession than TACOT while experiencing slightly higher wall temperatures, based on Fig. 6a, 6b, 7a, and 7b. Since the cork and void material do not go through pyrolysis, there is a distinct lack of modeled pyrolysis gases that circulate up stream and cool the solid matrix through to the boundary layer, which is the operating principle behind porous ablatives like PICA and TACOT [6]. It is plausible that since the cork is composed of carbon complexes, the cork reacts with the hot gases and chars, thereby removing heat from the flow through a chemical reaction and slowing the recession process. Comparatively, the carbon fiber preform is likely unable to go through a similar reaction, and so the solid matrix lacks the ability draw heat from the flow.

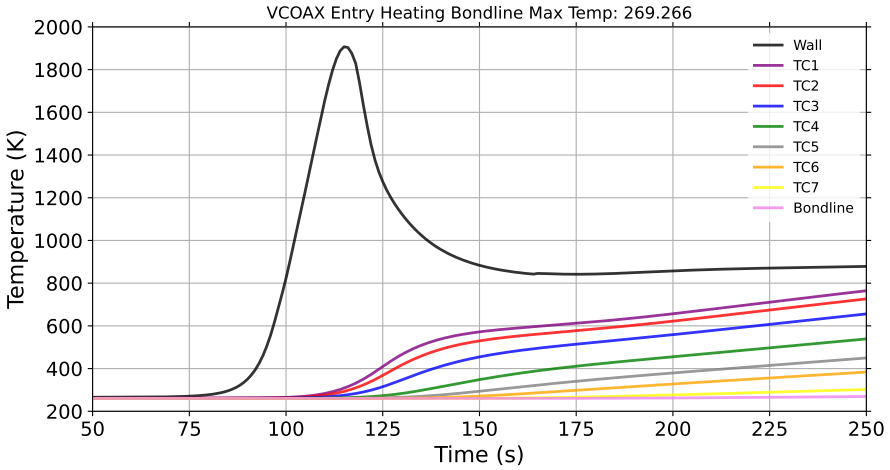

(a) Temperature profile of a 2.75 cm thick Cork heatshield during Venus Atmospheric Entry. The thermocouples are placed at depths of 1.5599, 1.5965, 1.6696, 1.8159, 1.9622, 2.1085 and 2.401 cm from the surface of the heatshield. The boundary condition and bond line temperature are also plotted.

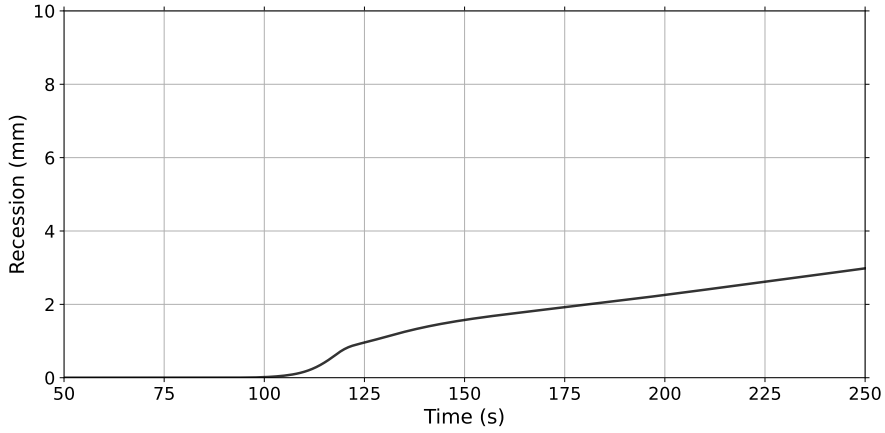

(b) Recession of a 2.75 cm thick Cork heatshield during Venus Atmospheric Entry.

Fig. 7 Performance of a cork heat shield during Venus atmospheric entry showing (a) temperature and (b) recession.

3. Novel Fiberglass-Based Material

In order to develop the workflow for integrating PuMA and PATO, a novel material based on fiberglass was created as detailed in Section III.D. As previously discussed, there were a variety of liberties taken in order to get a material file that could be run, resulting in a non-physical material. The list of conductivities at various temperatures used is outlined in Table 2. It is important to note that the conductivity values were extrapolated beyond the melting point of fiberglass, but is representative of what the thermal conductivity might be if a material like fiberglass could survive at much higher temperatures. The values for conductivity that were calculated using Eq. 1 were orders of magnitude higher than those of TACOT, and this is likely due to the estimated extinction coefficient.

Table 2 Extrapolated Fiberglass Material Properties.

Fiberglass Properties		
Temp (K)	k_{solid} (W/mK)	k_{eff} (W/mK)
2.42E+02	0.1470176349	4.267582E+02
2.56E+02	0.1479679335	5.053569E+02
2.70E+02	0.1495987508	5.930187E+02
2.84E+02	0.1512062289	6.893346E+02
2.97E+02	0.1533509854	7.944746E+02
3.11E+02	0.1548184406	9.109798E+02
3.66E+02	0.163703244	1.486875E+03
4.91E+02	0.1803888532	3.580712E+03
6.16E+02	0.1970744624	7.060170E+03
7.40E+02	0.2137600715	1.227714E+04
8.65E+02	0.2304456807	1.958353E+04
9.90E+02	0.2471312899	2.933124E+04
1.11E+03	0.263816899	4.187215E+04
1.24E+03	0.2805025082	5.755817E+04
1.36E+03	0.2971881174	7.674120E+04
1.49E+03	0.3138737265	9.977313E+04
1.61E+03	0.3305593357	1.270059E+05
1.74E+03	0.3472449449	1.587913E+05
1.86E+03	0.363930554	1.954813E+05
1.99E+03	0.3806161632	2.374278E+05
2.11E+03	0.3973017724	2.849828E+05
2.24E+03	0.4139873815	3.384980E+05
2.36E+03	0.4306729907	3.983254E+05
2.49E+03	0.4473585999	4.648168E+05
2.61E+03	0.464044209	5.383243E+05
2.74E+03	0.4807298182	6.191996E+05
2.86E+03	0.4974154274	7.077948E+05
2.99E+03	0.5141010365	8.044616E+05
3.11E+03	0.5307866457	9.095519E+05
3.23E+03	0.5474722549	1.023418E+06
3.36E+03	0.564157864	1.146411E+06

Unsurprisingly, this file yielded results that were essentially meaningless, but the code did run without errors producing the plots shown in Fig. 8. Since the bondline temperature is calculated at the interface between the heatshield material and the bondline boundary it is likely that PATO was able to come up with a temperature, but due to the extrapolation in the porousMat properties, was not able to do the same for the fiberglass material. As a result, none of the other thermocouples were plotted, including the wall temperature, and the bondline temperature and recession profile were much lower than what would be expected for a material with such high thermal conductivities.

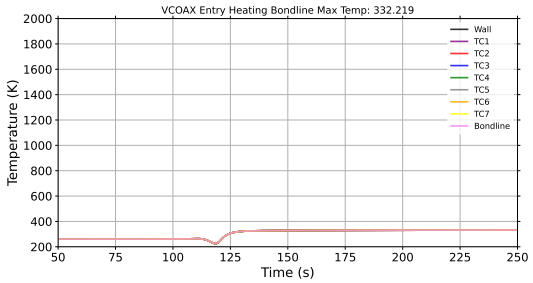

(a) Temperature profile of a 2.75 cm thick Fiberglass-based heatshield during Venus Atmospheric Entry. Only the bondline temperature successfully plotted.

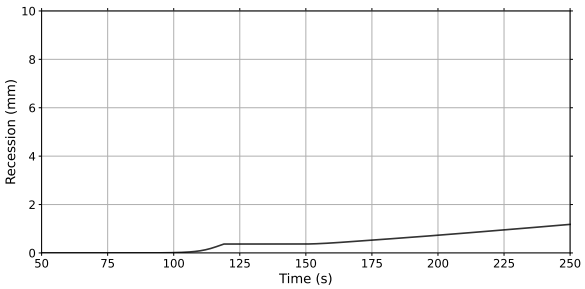

(b) Recession of a 2.75 cm thick Fiberglass heatshield during Venus Atmospheric Entry.

Fig. 8 Performance of a TACOT heat shield during Venus atmospheric entry showing (a) temperature and (b) recession.

V. Additional Limitations & Future Work

A. Atmospheric Model Limitations

An important caveat in these calculations is that the chemistry used by PATO is for the Earth's atmosphere, not Venus. In the AMAT calculations, the atmospheric trajectory was calculated using the Venus atmospheric density, temperature and pressure data already included within AMAT. However, within PATO, ablation and recession are calculated using the chemical reactions occurring at the interface between the atmosphere and the heat shield. As a result, the composition of the atmosphere will have an impact on reaction rates such as how quickly oxidation may occur.

After combing through files within the PATO environment, raw data for Earth and Mars environments were found, however only the Earth environment had been implemented as "B Prime" values usable by PATO as the surface chemistry on the TPS. The raw data file contains the boundary layer edge chemical composition which would be fairly simple to implement for Venus, however after speaking with some of the developers it was determined that calculating the B Prime values is a non trivial task, and likely has never been done for Venus. Since the trajectory in AMAT was calculated using Venus' atmospheric profile, the heat flux and temperature boundary conditions will be accurate, but it is likely that our recession will be slightly different from what it should be. The Venus atmosphere is 96.5% carbon dioxide and 3.5% nitrogen, with minor amounts of sulfur dioxide, argon, water, carbon monoxide, helium and neon [12]. It is expected that recession by both nitridation and oxidation will still occur, as the CO_2 is likely to dissociate across the shock, producing oxygen. It is not easy to determine how this may impact the recession without actually doing the calculation, but considering Earth's atmosphere is approximately 78% nitrogen and 21% oxygen[13], if all of the CO_2 is dissociated across the shock, the recession would likely be higher for the same entry heating conditions but Venus atmospheric chemistry. Further work would be required to validate this.

B. Virgin vs. Char Data

Another major caveat to mention is that PATO simulates ablation and recession by distinguishing the thermal conductivity of the virgin material from the char material. In the simplified analysis performed for the scope of this project, the effect of the phenolic charring was not determined, which is certainly a limitation in the analysis as there were significant differences between the virgin and char conductivity and emissivity for the preset TACOT material already implemented in PATO.

In future work, as new and more physical materials are investigated, a determination of the effective conductivity in both the virgin material and char would be necessary. By doing so, any simulations run will be more accurate and better reflect the true ablation process occurring.

C. Preform Geometries

This heatshield design process was limited in scope by only considering the microstructure existent in FiberForm, a carbon fiber preform composed of a random network of microscale fibers which underlies TACOT. This investigation

solely explored that effect that changing material properties, namely emissivity and thermal conductivity, have on the recession profile of the material sample. Nonetheless, it is recognized that the microstructure of the sample also plays a large role in the performance of the heatshield. To conduct a more thorough investigation, the microstructure shall be accounted for when selecting alternative materials.

In future work, other physical materials with distinctly different microstructure (e.g., spherical particle matrices and weaves) will be investigated. Notable examples of these two structures that have demonstrated high levels of performance in reentry conditions include P50 cork ablator and NASA's Heat shield for Extreme Entry Environment Technology (HEEET)[14].

VI. Conclusion

It is clear from the results of this investigation that developing the requirements for a heat shield is a non-trivial task and requires integration of multiple simulation codes as well as verification with experimental data. Based on the simplified calculations used, it would make the most sense to use the cork as a heat shield material. It has significantly better performance with a comparable if not lower density to PICA, which would help to decrease the overall spacecraft mass.

Acknowledgments

We would like to acknowledge Joseph Ferguson and Jeremie Meurisse for their support throughout the semester on this project.

References

[1] Council, N. R., *Vision and Voyages for Planetary Science in the Decade 2013-2022*, The National Academies Press, Washington, DC, 2011. https://doi.org/10.17226/13117, URL https://nap.nationalacademies.org/catalog/13117/vision-and-voyages-for-planetary-science-in-the-decade-2013-2022.

[2] Girija, A. P., Saikia, S. J., Longuski, J. M., and Cutts, J. A., "AMAT: A Python package for rapid conceptual design of aerocapture and atmospheric Entry, Descent, and Landing (EDL) missions in a Jupyter environment," *Journal of Open Source Software*, Vol. 6, No. 67, 2021, p. 3710. https://doi.org/10.21105/joss.03710, URL https://joss.theoj.org/papers/10.21105/joss.03710.

[3] Edquist, K., Dyakonov, A., Wright, M., and Tang, C., "Aerothermodynamic Design of the Mars Science Laboratory Heatshield," *41st AIAA Thermophysics Conference*, American Institute of Aeronautics and Astronautics, San Antonio, Texas, 2009. https://doi.org/10.2514/6.2009-4075, URL https://arc.aiaa.org/doi/10.2514/6.2009-4075.

[4] Prabhu, D., and Saunders, D., "On Heatshield Shapes for Mars Entry Capsules," *50th AIAA Aerospace Sciences Meeting including the New Horizons Forum and Aerospace Exposition*, American Institute of Aeronautics and Astronautics, Nashville, Tennessee, 2012. https://doi.org/10.2514/6.2012-399, URL https://arc.aiaa.org/doi/10.2514/6.2012-399.

[5] Way, D. W., Powell, R. W., Chen, A., Steltzner, A. D., Martin, A. M. S., Burkhart, P. D., and Mendeck, G. F., "Mars Science Laboratory: Entry, Descent, and Landing System Performance," *2007 IEEE Aerospace Conference*, IEEE, Big Sky, MT, USA, 2007, pp. 1–19. https://doi.org/10.1109/AERO.2007.352821, URL http://ieeexplore.ieee.org/document/4161337/.

[6] Lachaud, J., and Mansour, N. N., "Porous-Material Analysis Toolbox Based on OpenFOAM and Applications," Vol. 28, No. 2, 2014, pp. 191–202. https://doi.org/10.2514/1.T4262, URL https://arc.aiaa.org/doi/10.2514/1.T4262.

[7] Ferguson, J. C., Panerai, F., Borner, A., and Mansour, N. N., "PuMA: The porous microstructure analysis software," *SoftwareX*, Vol. 7, 2018, pp. 81–87.

[8] Ferguson, J. C., Semeraro, F., Thornton, J. M., Panerai, F., Borner, A., and Mansour, N. N., "Update 3.0 to "PuMA: The Porous Microstructure Analysis software",(PII: S2352711018300281)," *SoftwareX*, Vol. 15, 2021, p. 100775.

[9] Levinson, R., Akbari, H., and Gartland, L., "Impact of the temperature dependency of fiberglass insulation R-value on cooling energy use in buildings," 1996.

[10] Claucherty, S., and Sakaue, H., "Phenol-Formaldehyde Resin for Optical-Chemical Temperature Sensing," 2018. https://doi.org/10.3390/s18061756, URL www.mdpi.com/journal/sensors.

[11] Wright, M. J., Beck, R. A. S., Edquist, K. T., Driver, D., Sepka, S. A., Slimko, E. M., and Willcockson, W. H., "Sizing and Margins Assessment of Mars Science Laboratory Aeroshell Thermal Protection System," Vol. 51, No. 4, 2014, pp. 1125–1138. https://doi.org/10.2514/1.A32579, URL https://arc.aiaa.org/doi/10.2514/1.A32579, publisher: American Institute of Aeronautics and Astronautics.

[12] Williams, D., "Venus Fact Sheet," https://nssdc.gsfc.nasa.gov/planetary/factsheet/venusfact.html, 2021.

[13] National Geographic Society, "Atmosphere | National Geographic Society," https://www.nationalgeographic.org/encyclopedia/atmosphere/, 2019.

[14] Gasch, M., "Heatshield for Extreme Entry Environment Technology (HEEET) Thermal Protection System (TPS)," , 2019. URL https://www.ntrs.nasa.gov/api/citations/20190031968/downloads/20190031968.pdf.